Application of positive matrix factor analysis in heterogeneous kinetics studies utilizing the mixed-phase relative rates technique

Y. Liu, S.-M. Li and J. Liggio*

Air Quality Processes Research Section, Environment Canada, Toronto, M3H 5T4, Canada

*Corresponding author. Phone: 1-416-739-4840; fax: 1-416-739-4281;
E-mail: John.Liggio@ec.gc.ca

Abstract:

The mixed-phase relative rate approach for determining aerosol particle organic heterogeneous reaction kinetics is often performed utilizing mass spectral tracers as a proxy for particle phase reactant concentration. However, sometimes this approach may be influenced by signal contamination from oxidation products during the experiment. In the current study, the mixed-phase relative rates technique has been improved by combining a Positive Matrix Factor (PMF) analysis with electron ionization Aerosol Mass Spectrometry (unit mass resolution), thereby removing the influence of m/z fragments from reaction products on the reactant signals. To demonstrate the advantages of this approach, the heterogeneous reaction between OH radicals and citric acid (CA) was investigated using a photochemical flow tube coupled to a compact time-of-flight aerosol mass spectrometer (C-ToF-AMS). The measured heterogeneous rate constant (k_2) of citric acid toward OH was $(3.31\pm0.29)\times10^{-12}$ cm^3 $molecule^{-1}$ s^{-1} at 298 K and (30±3) % RH and was several times greater than the results utilizing individual m/z fragments. This phenomenon was further evaluated for particulate-phase organophosphates (TPhP, TDCPP, and TEHP), leading to k_2 values significantly larger than previously reported. The results suggest that heterogeneous kinetics can be significantly underestimated when the structure of the products is highly similar to the reactant and when a non-molecular tracer is measured with a unit mass resolution aerosol mass spectrometer. The results also suggest that the heterogeneous lifetime of organic aerosol in models can be overestimated due to underestimated OH uptake coefficients. Finally, a comparison of

reported rate constants implies that the heterogeneous oxidation of aerosols will be dependent upon a number of factors related to the reaction system, and that a single rate constant for one system cannot be universally applied under all conditions.

1. Introduction

Reaction kinetics data provide key parameters for both air quality and climate models. They are required to compute the trace gas and particle matter (PM) content of the atmosphere (Kolb et al., 2010) and to evaluate the atmospheric lifetime and fate for individual species. Organic particles make up 10-90 % of the global submicron particle mass in the lower troposphere (Zhang et al., 2011), and is comprised of various reactive organic species, which are subject to atmospheric heterogeneous oxidation. Previous studies have found that heterogeneous reactions with OH in particular, can lead to an increase in density, CCN activation (George and Abbatt, 2010) and optical extinction (Cappa et al., 2011) of organic particulate matter. Therefore, there is a growing interest in understanding not only the mechanism of PM transformation through heterogeneous reactions including oxidation, but also determining the rates at which organic aerosols are chemically transformed in the atmosphere.

To this end, Donahue et al. (Donahue et al., 2005) and Hearn and Smith (Hearn and Smith, 2006) developed a mixed-phase relative rate technique for measuring organic PM component heterogeneous reaction kinetic rate constants. In this method, the rate constant of the compound of interest is determined from the decrease of its particle phase relative concentration as a function of oxidant exposure. The oxidant levels are simultaneously estimated via the measured loss of a gas phase reference compound after applying the known second-order rate constant (k_2) toward the oxidant. In this approach the rates of chemical change are given by,

$$-\frac{\mathrm{d}c_{\mathrm{A}}}{\mathrm{d}t} = k_{2,\mathrm{A}} c_{\mathrm{A}} c_{\mathrm{Ox}} \quad (1)$$

$$-\frac{\mathrm{d}c_{\mathrm{R}}}{\mathrm{d}t} = k_{2,\mathrm{R}} c_{\mathrm{R}} c_{\mathrm{Ox}} \quad (2)$$

where c_{A}, c_{R} and c_{Ox} are the particle phase concentration of the compound of interest (A), the gas phase concentration of the reference compound (R) and oxidant (molecules cm^{-3}) respectively, while $k_{2,\mathrm{A}}$ and $k_{2,\mathrm{R}}$ are the second-order rate constant of A and R to the oxidant (cm^3 $molecule^{-1}$ s^{-1}). A relative rate constant (k_{r}) (ie: particle phase reaction rate of A, relative to the gas phase rate of R) can be derived by dividing Eq. (1) by Eq. (2). The derivation of k_{r} provides a means to obtain heterogeneous kinetic data without the need to know the absolute concentration of the oxidant. The differential and integral forms for the relative rates technique are shown as Eq. (3) and (4),

$$\frac{\mathrm{d}c_{\mathrm{A}}}{c_{\mathrm{A}}} = \frac{k_{2,\mathrm{A}}}{k_{2,\mathrm{R}}} \frac{\mathrm{d}c_{\mathrm{R}}}{c_{\mathrm{R}}} = k_{\mathrm{r}} \frac{\mathrm{d}c_{\mathrm{R}}}{c_{\mathrm{R}}} \quad (3)$$

$$\log \frac{c_{\mathrm{A}}}{c_{\mathrm{A},0}} = k_{\mathrm{r}} \log \frac{c_{\mathrm{R}}}{c_{\mathrm{R},0}} \quad (4)$$

from which the relative rate constant (k_{r}), is the slope of the line derived by plotting the logarithmic relative concentration of A against that of R (relative to initial conditions; $c_{\mathrm{A},0}$). The second-order heterogeneous rate constant of the compound of interest ($k_{2,\mathrm{A}}$) towards the oxidant may then be calculated using the obtained k_{r} and the known $k_{2,\mathrm{R}}$ (ie:$k_{2,\mathrm{A}} = k_{\mathrm{r}} \times k_{2,\mathrm{R}}$).

Using this method, a number of studies have quantified the uptake coefficients of O_3, OH, Cl, and NO_3 on various organic particles, and the corresponding second order rate constants for the degradation of organic compounds (Hearn and Smith, 2006;George et al., 2007;Lambe et al., 2007;McNeill et al., 2007;McNeill et al.,

2008;Smith et al., 2009;Kessler et al., 2010;Renbaum and Smith, 2011;Kessler et al., 2012;Liu et al., 2012;Sareen et al., 2013).

Although gas chromatograph mass spectrometry (GC-MS) has been widely used in the kinetics studies (Weitkamp et al., 2008a;Weitkamp et al., 2008b;Lambe et al., 2009;Isaacman et al., 2012), quantifying the particle phase loss of an organic compound in such studies often relies upon aerosol mass spectrometry techniques to monitor specific particle phase reactant ions of interest in semi-real time. Aerosol mass spectrometry instruments utilizing high resolution detection and soft ionization techniques, such as chemical ionization (Aerosol CIMS) (Hearn and Smith, 2006;McNeill et al., 2007;McNeill et al., 2008;Renbaum and Smith, 2011;Sareen et al., 2013) and vacuum ultraviolet photo-ionization (VUV-ATOFMS)(Liu et al., 2012), have been utilized to measure the concentration of the target organic compounds in particles. However, Aerosol Time-of-Flight or Quadrupole Mass Spectrometry (ToF-AMS or Q-AMS) employing electronic ionization (EI; 70 eV) as an ion source remains the prevalent instrument used in such organic particle experiments. In utilizing this approach, a specific fragment (usually the fastest-decaying ions in the spectrum) is often chosen as a tracer for the particle phase compound of interest. For example, m/z 297 has been selected as a tracer for bis(2-ethylhexyl) sebacate (BES) (George et al., 2007), m/z 71 for hexacosane (Lambe et al., 2007), m/z 113 for squalane (Smith et al., 2009), m/z 104 and 144 for erythritol and levoglucosan (Kessler et al., 2010), and m/z 152, 68 and 98 for 1,2,3,4-butanetetracarboxylic acid, citric acid and tartaric acid (Kessler et al., 2012) respectively.

However, the use of EI in conjunction with a particle vaporizer in the AMS results in heavy fragmentation for organic compounds due to the high energy associated with the EI source (70 eV) and the high temperature (~873 K) of the vaporizer (Jayne et al., 2000;Allan et al., 2003). Under such conditions, the tracer m/z fragment is prone to interferences due to (1) the fragmentation of larger ions and/or molecules and (2) fragments from particle phase oxidation products. Both can contribute to the tracer m/z signal, sometimes leading to an insensitive or nonlinear response of the tracer m/z to the concentration of the target reactant during oxidation. The same may also be true for the m/z for the molecular ion should one exist. In particular, it is true if the structure of the product is highly similar to the reactant and when the tracer is measured with a unit-mass resolution (UMR) aerosol mass spectrometer. Although it is often assumed that the chosen tracer ion does not contribute significantly to the mass spectra of any possible oxidation products or vice versa (Kessler et al., 2010), this is not always the case. In our previous work, we observed that the magnitude of the second order heterogeneous rate constant (k_2) increases as a function of increasing m/z of the fragment chosen as a tracer of the parent molecule (Liu et al., 2014). The same trend has also been observed for the OH oxidation of ambient biogenic secondary organic aerosol (SOA) (Slowik et al., 2012). This suggests an interference from the fragments selected, and points to the necessity to separate the signals of the compound of interest, from other compounds (products and/or fragment) for kinetic studies.

In the current study, we improve the mixed-phase relative rate technique used for

studies of the heterogeneous oxidation of organic aerosol (OA) using positive matrix factorization (PMF) analysis of UMR-AMS derived kinetic data. Heterogeneous kinetics of citric acid (CA) toward OH oxidation was studied in a photo-chemical flow tube coupled to an Aerodyne C-ToF-AMS and an Ionicon Analytik High Resolution Proton Transfer Reaction Mass Spectrometer (PTR-ToF-MS). As it was applied to heterogeneous oxidation of ambient biogenic SOA (Slowik et al., 2012), PMF analysis was used to successfully deconvolve the full mass spectra of the reactant from the potential oxidation products, hence allowing proper accounting of the time evolution of reactant concentrations during photochemical oxidation.

2. EXPERIMENTAL DETAILS

2.1 Flow tube experiments. A detailed schematic representation of the experimental system utilized in this study has been described elsewhere (Liu et al., 2014). Briefly, organic particles (citric acid) were generated via atomization (model 3706, TSI), dried through a diffusion drier and size-selected with a differential mobility analyzer (DMA) (model 3081, TSI). The dried, monodispersed CA particles were introduced into the flow tube reactor and exposed to differing OH concentrations. OH radicals were produced by the photolysis of O_3 at 254 nm in the presence of water vapor. O_3 was generated by passing zero air through an O_3 generator (OG-1, PCI Ozone Corp.). The O_3 concentration in the reactor was measured using an O_3 monitor (model 205, 2B Technologies) and ranged from 0-1000 ppbv. Relative humidity (RH) in the reactor was held constant (30±3) % by varying the ratio of wet to dry air used as an air source, and was measured at the exit of the flow tube reactor. The temperature was held

176 constant at 298 K by circulating a temperature controlled fluid through the outer
177 jacket of the reactor. The residence time in the flow reactor was 52 s. The steady-state
178 OH exposures were varied from 0 to ~7.0×10^{11} molecules cm^{-3} s which was estimated
179 on the basis of the decay of methanol from (as a reference compound) its reaction
180 with OH. The decay of methanol from its reaction with OH was measured using the
181 PTR-ToF-MS. The k_2 of methanol, 9.4×10^{-13} cm^3 $molecule^{-1}$ s^{-1}, was used for the OH
182 exposure calculation (Atkinson and Arey, 2003).

183 OH radical reactions were performed in a custom-made reactor consisting of two
184 electro-polished stainless steel cylinders with inner diameter of 7.3 cm. The first stage
185 contained static mixing elements (StaMixCo) to ensure that particles and gas phase
186 species were well mixed prior to entering the reaction region (second stage). Fluid
187 dynamics simulations of the flow tube confirmed that particles and gas phase species
188 were well mixed in the reactor, with a uniform initial velocity profile. The size and
189 composition of the particles exiting the reactor were measured by a scanning mobility
190 particle sizer (SMPS, TSI) and an Aerodyne C-ToF-AMS (Drewnick et al., 2005)

191 Control experiments demonstrated that O_3 or 254 nm light exposure did not lead
192 to the decomposition of CA. Analytic grade CA (EM, Germany) was used as received.
193 18.2 MΩ water was used as solvent.

194 **2.2 PMF analysis and kinetics calculation**.

195 PMF is a multivariate factor analysis tool that decomposes a matrix of speciated
196 sample data into two matrices, namely, factor contributions and factor profiles
197 (Paatero and Tapper, 1994), such that

198 $x_{ij} = \sum_p g_{ip} f_{pj} + e_{ij}$ (5)

199 Where i and j refer to row and column indices in the matrix, respectively, p is the
200 number of factors in the solution, x_{ij} is an element of the $m \times n$ matrix $\boldsymbol{X}$ of measured
201 data elements to be fit, and e_{ij} is the residual. Results are constrained so that no
202 sample can have a negative source contribution. The PMF solution minimizes the
203 object function Q (Eq.6), based upon the uncertainties (u) (Norris and Vedantham,
204 2008).

205 $Q = \sum_{i=1}^{n} \sum_{j=1}^{m} \left(\frac{e_{ij}}{u_{ij}}\right)^2$ (6)

206 Its ability to separate the signals of a multi-component matrix has been well
207 established. PMF analysis has been widely used for source apportionment of ambient
208 particles in field measurements (Song et al., 2006;Yuan et al., 2006;Viana et al.,
209 2008;Ulbrich et al., 2009;Liggio et al., 2010;Schwartz et al., 2010). Three secondary
210 organic aerosol factors (SOA1, SOA2, SOA3) have been identified for OH initiated
211 oxidation of laboratory SOA (George and Abbatt, 2010). Similarly, SOA factors have
212 also been successfully isolated in OH oxidation of ambient biogenic SOA (Slowik et
213 al., 2012). Therefore, the use of PMF for separating the reactants from the products in
214 laboratory studies aimed at using the relative rates method for heterogeneous kinetic
215 studies would seem to be a reasonable approach.

216 The AMS data for CA oxidation from all experiments combined were used as
217 input into the PMF Evaluation Toolkit (PET) v2.05 (Paatero, 1997;Paatero and Tapper,
218 1994;Ulbrich et al., 2009) to separate the signals of CA and the corresponding
219 oxidation products. In the AMS data, the m rows of $\boldsymbol{X}$ are ensemble average mass

spectra (MS) of typically tens of thousands of particles measured over each averaging period (typically 2 min) and the n columns of $\boldsymbol{X}$ are the time series (TS) of each m/z sampled.

PMF analyses were done in the robust mode. The default convergence criteria were not modified. The Q values as a function of FPEAK from -1 to +1 were examined (Reff et al., 2007). For the variables with signal-to-noise ratio (SNR) less than 0.2 ("bad" variables) and downweight variables with SNR between 0.2 and 2 ("weak" variables), their error estimates were increased by a factor of 10 and 3, respectively, as recommended by Paatero and Hopke (Paatero and Hopke, 2003). In this study, the SNR of all m/z fragments are larger than 0.2. The error values for m/z 44, 18, 17 and 16 were multiplied by sqrt(4).

The extracted factor profiles (mass spectra for CA and the oxidation products) were compared with the NIST mass spectrum of pure CA and that measured with the C-ToF-AMS directly via atomization. The temporal concentration profiles (factor contributions) of CA were further confirmed via comparison to the known experimental conditions used for kinetics calculations (ie: zero OH exposure should result in a CA factor contribution of 100 %). For comparison with the PMF results, the kinetic rate constants (k_r) were also calculated using specific individual tracers of CA at m/z 87, 129 and 147, separately. The k_r of CA toward methanol was calculated according to Eq. (4). The k_2 of CA was further calculated with the known k_2 of methanol and k_r.

The reactive uptake coefficient of OH (γ_{OH}) with CA was calculated using the

following formulation (Kessler et al., 2010;Worsnop et al., 2002;Kessler et al., 2012;Liu et al., 2012):

$$\gamma_{OH} = \frac{2D_p \rho_{CA} N_A}{3 v_{OH} M_{CA}} \varphi k_2 \qquad \text{Eq (7)}$$

Where D_p is the surface-weight average particle diameter of unreacted particles (cm), ρ_{CA} is the density of CA (g cm^{-3}), N_A is Avogadro's number, v_{OH} is the average speed of OH radicals in the gas phase (cm s^{-1}), M_{CA} is the molecular weight of CA (g mol^{-1}), φ is a correction factor for diffusion of OH from the gas phase to particle phase.

3.0 Results

3.1 PMF analysis of AMS data.

To ensure that oxidation of CA in particles does not result in a PTR-ToF-MS response for methanol in the gas phase (thus compromising the OH radical reference measurement), the oxidation of pure CA was performed in the absence of methanol, with no gas phase methanol signal detected by the PTR-ToF-MS. The mass concentration of the OA measured with the AMS during oxidation is shown in Figure 1A, which was constant. The results of Figure 1A demonstrate that the aerosol source is adequately stable for kinetic studies to be performed.

A two factor solution from the PMF analysis accounts for 99.98 % of the variance of the data. When the number of factors is greater than 2, none of the obtained factors resembles that of pure CA, whose contribution should be approximately 100 % when OH is absent in the reactor. Figures 1B and C represent the temporal variations of the typical 2-factor PMF solution of AMS data when CA is

exposed to varying OH concentrations. The error bars indicate the rotational uncertainty in the PMF analysis. Three independent experiments were performed to test the response of CA signal to OH exposure (determined by O_3 concentration). In the first and the third experiments, OH exposure was stepped downwards (high to low OH) by changing the power of O_3-generator with the same flow rate and RH, while the inverse sequence was performed in the second experiment.

As demonstrated in Figure 1B and C, in the absence of OH radical (labeled“0”), factor 1 (Figure 1B) accounts for (94.7±0.9) % of the OA mass, while factor 2 (Figure 1C) contributes (6.2±0.7) % of OA. This is consistent with the experimental conditions of zero OH radical (ie: no oxidation), and suggests that factor 1 should be assigned to the citric acid reactant. Impurities in the CA or the water used to atomize CA likely contributed to factor 2. When OH exposure was decreased in a step-wise manner in the first and the third experiment (Figure 1B), the extracted factor representative of CA (factor 1) increased synchronously, and is accompanied with a decrease in factor 2. Therefore, factor 2 is interpreted as the OH oxidation products of CA. This is consistent with the second experiment, where the inverse trend was observed with a step-wise OH exposure increase. Based upon this evidence, we conclude that changes in the time series of factors 1 and 2 extracted by PMF are consistent with the expected response to OH exposures, namely, that higher OH exposure resulted in a decrease in CA (factor 1) and an increase in the oxidation products (factor 2).

The factor profiles (ie: mass spectra) extracted by PMF analysis are shown in

Figure 2. The main fragments of CA including m/z values 129 ($C_5H_5O_4^+$) and 87 ($C_3H_3O_3^+$) are present in factor 1 (Figure 2A). These fragments are in good agreement with the NIST mass spectra of pure CA and the mass spectrum of pure CA particles measured with the C-ToF-AMS (Figure 3). Figure 4 further compared the normalized mass spectra of factor 1 and pure CA directly measured with the C-ToF-AMS. The relative intensities for all ions of pure CA are linearly correlated with that of factor 1 with a slope of 0.985 and R of 0.9999. This further confirmed that factor 1 should be assigned to unreacted CA. Figure 2C shows the difference mass spectra (factor 2 – factor 1). Consumption of m/z values 147 ($C_5H_7O_5^+$), 129, 87, 85 ($C_4H_5O_2^+$) and 60 ($C_2H_4O_2^+$) can be observed, which is consistent with the assignment that factor 2 belongs to oxidation products of CA. However, small changes in the relative intensities of these peaks suggest that the structure of the oxidation products of CA are likely similar to that of CA. For example, as shown in Figure 2A and B, the intensity of m/z 129 and 87 in factor 2 are 0.0125±0.0046 and 0.0218±0.0013 compared to 0.0141±0.0046 and 0.0235±0.0013 in factor 1.

The changes of the relative concentrations of gas phase methanol and particle phase CA are shown in Figure 5. The signal of CA extracted by PMF analysis also responded to OH exposure as expected, when methanol was present in the gas phase, which is similar to that of Figure 1. The relative intensities of the typical tracers of CA at m/z 87, 129 and 147 are shown in Figure 5C. As shown in Figure 5 B and C, the drop in the PMF product factor is substantially greater than that of any of the individual ions. In addition, the consumption of the smaller tracer (m/z 87) is

substantially lower than that of the larger ones (m/z values 129 and 147). For example, the maximum consumption of CA extracted with PMF analysis is approximately 80 %, in comparison to ~30 %, ~10 % and 5 % for m/z values 147, 129 and 87, respectively. These results support the small differences in the mass spectra between the unreacted CA and its oxidation products as shown in Figure 2. Furthermore, it suggests that the measured loss of these fragments, which were supposedly only derived from CA, had in fact contributions from the fragmentation of the products of CA oxidation. This ultimately would lead to an underestimation of the second order heterogeneous rate constant (or OH uptake coefficients) if these fragments were chosen as the proxies for the particle phase concentration of CA. In particular, the difference between the PMF-factor decay rate and the marker-ion decay rate is mathematically possible only when the two factors (reactants and products) are extremely similar.

3.2 Reaction kinetics. The saturation vapor pressure of CA at 298K is 1.6×10^{-7} Pa (Huisman et al., 2013), thus 99.9% of CA should be present in the particle phase under the current experimental conditions according to a partition model (Kroll and Seinfeld, 2008;Pankow, 1994). Although new particle formation was observed with a CPC in the experiments (at the exit of the reactor), it has no influence on the measured mass concentration of OA due to the small particle size of the new particles. This is well supported by the constant mass concentration of OA measured with the AMS during oxidation experiments (Figure 1A). In addition, as pointed out in our previous work (Liu et al., 2014), evaporation of CA from particles could potentially contribute to the decreases in particle phase CA concentration observed as a function of OH

exposure. If CA evaporation was at play, the derived reaction rates will be overestimated using either the present approach or the simpler methods of using single fragments. The evaporation of CA from the particle phase under these experimental conditions from control experiments is less than 0.005 % based upon an evaporation model (Jacobson, 2005). This implies that the observed changes in CA concentration in the particle phase were due to the particle phase reaction.

The relative rates (relative to initial conditions) for CA and methanol in these experiments are shown in Figure 6. The logarithmic c/c_0 of CA both measured with the tracers and extracted with PMF analysis linearly correlated to that of methanol with $R^2>0.95$. The derived relative rate constant based upon PMF analysis is 3.01±0.27, while it is 0.72±0.05 and 0.22±0.01 for m/z values 147 and 129, respectively. Applying the k_2 value of methanol towards OH of 9.4×10^{-13} cm^3 $molecule^{-1}$ s^{-1} at 298 K (Atkinson and Arey, 2003), the k_2 of CA is calculated as $(2.83\pm0.25)\times10^{-12}$ using the PMF approach, or $(6.77\pm0.47)\times10^{-13}$ using the single tracer at m/z 147 and $(2.02\pm0.01)\times10^{-13}$ cm^3 $molecule^{-1}$ s^{-1} using the single tracer at m/z 129, respectively. The reaction between methanol and OH radicals occurs in the gas phase, while for the CA oxidation it occurs in particle phase. Thus it is necessary to correct for OH diffusion from the bulk gas phase to the particle phase. Applying a diffusion correction utilizing a previously developed empirical formula (Fuchs and Sutugin, 1970;Worsnop et al., 2002;Widmann and Davis, 1997), the diffusion-corrected k_2 is $(3.31\pm0.29)\times10^{-12}$ using the PMF approach, and $(7.92\pm0.55)\times10^{-13}$ and $(2.36\pm0.01)\times10^{-13}$ cm^3 $molecule^{-1}$ s^{-1} using single tracers at m/z

147 and 129, respectively. The diffusion-corrected γ_{OH} is calculated as 2.74±0.24 using the PMF approach, and 0.66±0.05 and 0.20±0.01 using single tracers at m/z 147 and 129, respectively. The γ_{OH} for a number of different organic particles have previously been measured, and are in the range of 0.3 – 2.0 (Kessler et al., 2010;George et al., 2007;Hearn and Smith, 2006;Lambe et al., 2007;Smith et al., 2009;Kessler et al., 2012). As pointed out by Hearn and Smith (2006), the large γ implies that secondary radical reactions within the particles could play a significant role in heterogeneous chemistry, particularly since gaseous citric acid in these studies is insignificant.

It should be pointed out that oxidant diffusion in the particle phase should lead to a concentration gradient of oxidant and a negative impact on reaction kinetics (Donahue et al., 2005). However, as shown in Figure 6, this effect is negligible under the current experimental conditions. Based upon the measured c/c_0 and the initial diameter of the CA particles, the maximum OH diffusion depth is approximately 25 nm. Given the residence time (τ) in this study (52 s), a significant OH concentration gradient will exist in particle phase if the D_{OH} in CA particles is smaller than 1.2×10^{-17} m^2 s^{-1} ($D=l^2/\tau$) (Donahue et al., 2005). At the present time, the D_{OH} in CA particles is unavailable. However, Price et al. (Price et al., 2014) have reported the diffusion of D_2O in several organics (sucrose and levoglucosan) to be larger than $\sim1\times10^{-16}$ m^2 s^{-1} even under dry condition. This implies that a gradient in OH concentration in the CA particles is negligible under the current conditions.

4. Discussion

Kessler et al. (Kessler et al., 2012) have reported the k_2 of CA toward OH to be $(4.3\pm0.8)\times10^{-13}$ cm^3 molecule s^{-1} at 308 K and 30 % RH with an Aerodyne HR-AMS. In their work, the diameter of particles and RH were equivalent to the current work, while their experimental temperature was 10 K higher. In addition, a m/z fragment of 68 was used as a tracer for CA in their work to derive the heterogeneous rate constant. Conversely, no significant consumption of m/z 68 was observed in the current study. The lack of a m/z 68 fragment consumption here may be explained by the choice of reaction conditions. In the work of Kessler et al., OH concentration exposure ($0\sim7\times10^{12}$ molecule cm^{-3} s) was approximately an order of magnitude higher than that reported here. Recent evidence suggests that the product distribution during OA oxidation greatly depends upon OH exposure levels (Wilson et al., 2012). Hence, it is possible that more oxidized products formed via multi-generational chemistry at high OH were formed, which may have less of an influence on the signal of the chosen tracer (m/z 68), and result in product AMS spectra which are significantly different than that of the reactant thus mitigating the use of PMF (which was not the case here). In studies of the OH oxidation of squalane (Sq) (Smith et al., 2009;Wilson et al., 2012), the first generation product (SqO) was the primary contributor to the products when the OH exposure was the same as the highest OH level in the current study (7.0×10^{11} molecules cm^{-3} s), while higher generation products were predominant at OH exposures was greater than $\sim2\times10^{12}$ molecules cm^{-3} s. Although not directly comparable, it is reasonable to assume that lower OH exposure in the current work should lead primarily to the first generation products, which are highly similar to CA.

However, the formation of multi-generation products cannot be completely ruled out. Secondly, the difference in OA and oxidant concentrations as well as timescale may also have an influence on the product distribution. Thirdly, a high resolution time-of-flight aerosol mass spectrometer (HR-ToF-AMS) was used in their work, while a C-ToF-AMS with unit-mass resolution was used in this study. The higher mass resolution of the HR-ToF-AMS relative to a C-ToF-AMS, may further reduce the influence of product fragments on m/z 68 (or others). Finally, differences in temperature or other reaction conditions between experiments may also have led to differences in the morphology of CA and subsequent differences in the reactivity of CA.

Given the above discrepancy in the consumption of m/z 68, the fragments at m/z 129 and 147 were used as tracers in this work. The measured k_2 of CA utilizing m/z 129 and 147 in this study is of the same order of magnitude as that reported in Kessler et al. (2012). However, as shown in Figure 3C, the consumption of m/z 87 is much lower than that of m/z 129. The apparent k_2 of CA based on m/z 87 is $(9.9\pm0.8)\times10^{-14}$ cm^3 $molecule^{-1}$ s^{-1}, and the diffusion-corrected k_2 is $(1.16\pm0.09)\times10^{-13}$ cm^3 $molecule^{-1}$ s^{-1}. This suggests that the derived rate constant greatly depends upon the size of the tracer fragment, with larger fragments resulting in larger values of k_2 in this study. This is consistent with previous work investigating the OH oxidation of tris-phenyl phosphate (TPhP) (Liu et al., 2014) and ambient biogenic SOA (Slowik et al., 2012). The k_2 of CA based upon PMF analysis is approximately an order of magnitude larger than the Kessler result measured with the tracer at m/z 68, and 4.2 times greater than

418 that calculated based upon m/z 147 in this study. The differences in product
419 distributions that may arise between this and the work of Kessler et al., consistent
420 with the fact that m/z 68 is not consumed in the current study, suggests that the PMF
421 approach was likely required in this work to separate similar product and reactant
422 spectra ultimately caused by lower OH exposure.

423 A number of factors may be responsible for the discrepancy between derived rate
424 constants. It has previously been observed that the presence of O_3 can inhibit the rate
425 of OH reaction, perhaps by reacting with OH radicals or by O_3 or intermediate species
426 blocking surface active sites (Renbaum and Smith, 2011). A Langmuir-Hinshelwood
427 mechanism has been observed for the reaction of O_3 on organic surfaces (Pöschl,
428 2005). It has also been demonstrated that a higher concentration of gas phase reactant
429 often leads to a lower uptake coefficient due to surface saturation (Ma et al., 2010 ;Li
430 et al., 2002). Differences in k_2 may also arise from the competition between reaction
431 products and reactants for available OH, or via the blocking or coating of the reactant
432 by products which would require liquid phase diffusion of OH to degrade the original
433 CA. In experiments with higher OH exposures (Kessler et al 2012) it is possible that
434 significantly more product mass is mixed and/or coated onto the original particle thus
435 decreasing the perceived k_2. Different timescales and concentrations of reactants
436 might also lead to different rate constants (Che et al., 2009). Finally, as pointed out
437 above, the differing reaction conditions may have led to a different CA morphology
438 and subsequent differences in the reactivity towards OH. The significant difference
439 between the reported rate constants highlights an important issue in heterogeneous

440 reactions of the atmosphere, and in the experiments trying to derive such kinetics. It
441 implies that the particle composition and/or morphology as determined by the reaction
442 conditions in the laboratory or the ambient atmosphere will have a large effect on the
443 OH kinetics.

444 Citric acid is a hydroxyl substituted poly carboxyl acid. Scheme 1 summarizes its
445 possible fragmentation pathways. The typical mass peaks including m/z 147, 129, 87,
446 85 and 68 would result from this scheme and were indeed observed. The fragments at
447 m/z 129, 87, 85 and 68 are also likely from CA oxidation products fragments, and
448 hence their signal intensities may be highly influenced by products and/or larger
449 fragments, in particular, when the oxidized products are highly similar to the reactant.
450 In some instances, oxidation products can exhibit similar fragmentation pathways as
451 the reactants. This is likely the case for the smaller fragments of CA. For example,
452 scheme 2 illustrates the possible fragmentation pathways of
453 2,3-dihydroxypropane-1,2,3-tricarboxylic acid, which is one of the possible products
454 from the OH oxidation of citric acid in terms of the general chemistry described by
455 Atkinson et al. (Atkinson, 1986). As observed in Scheme 2, there are several pathways
456 leading to the fragment at m/z 87, implying that the decrease in the signal of m/z 87
457 due to CA oxidation is likely to be compensated by fragments from the oxidation
458 products. In addition, it is also possible to form fragments with the same m/z as the
459 parent citric acid if the dehydration reaction (the 6th path in Scheme 2) takes place
460 initially. Other possible reaction products might also play similar roles in the
461 fragments. This is highly possible when the product distribution contains products

462 which are structurally similar to the reactant under low oxidant exposure conditions.

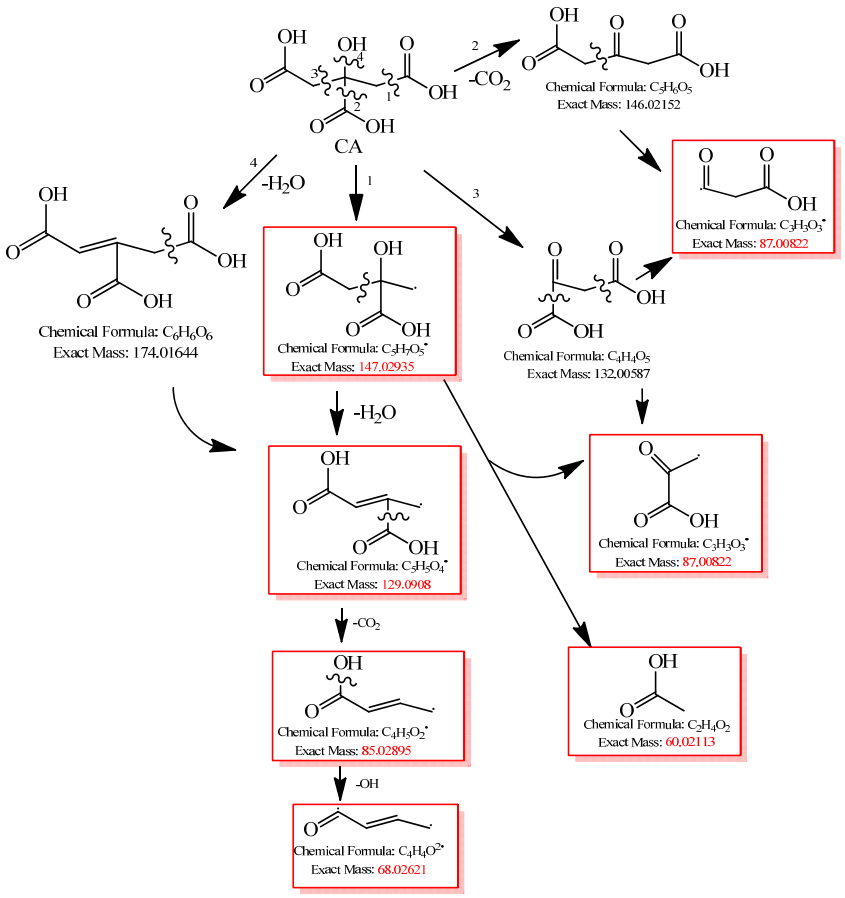

463

464 Scheme 1. Possible fragmentation pathways for citric acid.

465

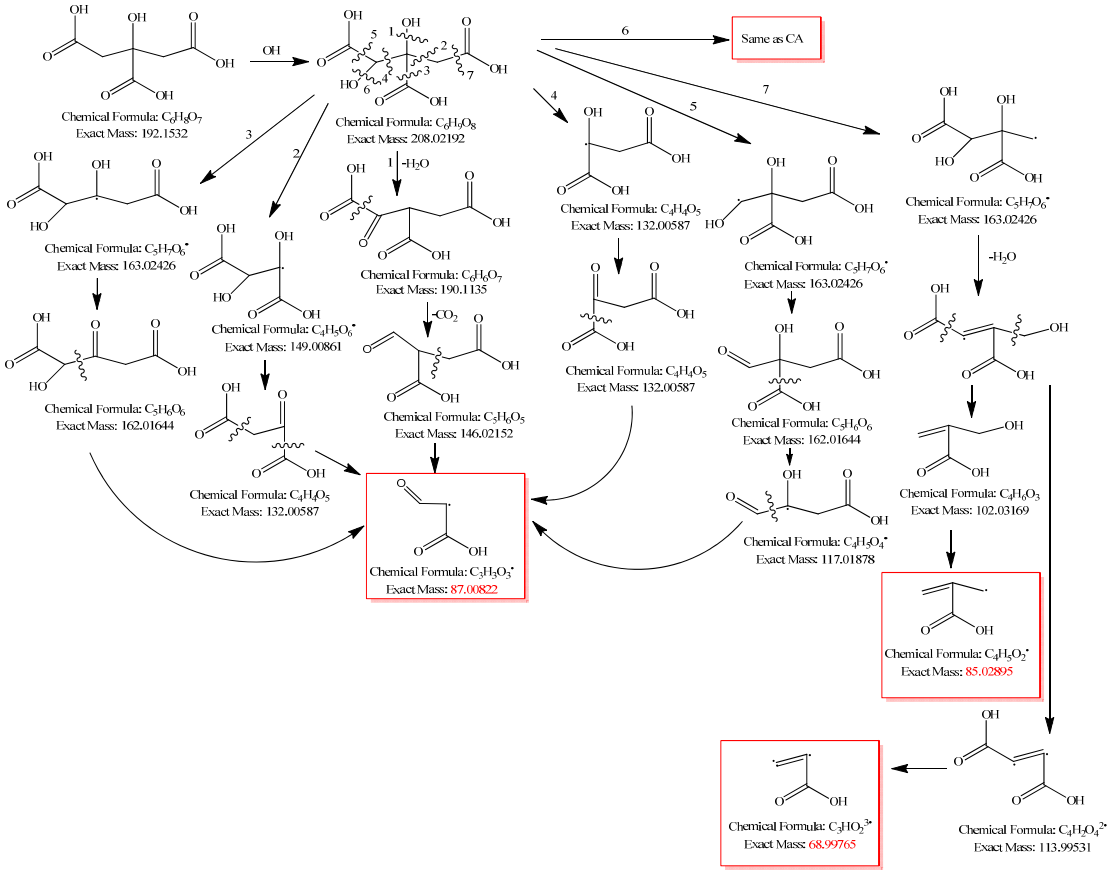

Scheme 2. Possible fragmentation pathways for an oxidation product of citric acid in terms of the general chemistry described by Atkinson et al. (Atkinson, 1986).

The current relative rate method based upon PMF analysis was used to re-analyze the heterogeneous oxidation kinetics of three organophosphate flame retardants found in ambient particles and reported previously (Liu et al., 2014). The k_2 values for TPhP, tris-1,3-dichloro-2-propyl phosphate (TDCPP) and tris-2-ethylhexyl phosphate (TEHP) utilizing the tracer and PMF approaches are summarized in Table 1. For TPhP, its molecular ion peak (M^+;326) was chosen as a tracer; while the largest detectable fragments, i.e. m/z 381 and 323, were chosen for TDCPP (M^+; 431) and TEHP (M^+;

435), respectively. The typical evolution of the PMF factors of TPhP, TDCPP, and TEHP are shown in Figures S1-3. For TPhP, the measured k_2 values derived by both methods are comparable within the experimental uncertainties, while k_2 of TDCPP and TEHP based upon PMF analysis is 1.5 and 1.6 times larger than that using the chosen tracers. The good agreement between methods for TPhP is likely due to the fact that the molecular ion peak (M^+) is measurable for TPhP with the AMS, while it is not observable for TDCPP, TEHP and CA. Therefore, the influence of secondary fragmentation from larger fragments has little influence on the signal of M^+ for TPhP. These results also demonstrate that a substantial underestimation of rate constants could result when a non-molecular ion tracer is used to monitor the particle phase concentration of organic matter with UMR-AMS for heterogeneous kinetic studies. The discrepancy between the tracer and PMF based methods for other compounds will depend upon a number of factors including: structure of products, OH exposure level, particle morphology, and organic species competing OH reactions.

5.0 Implications and Conclusions

The measured k_2 for citric acid toward OH is $(3.31\pm0.29)\times10^{-12}$ cm^3 $molecule^{-1}$ s^{-1} at 298 K and 30 % RH. This value is at least 4.2 times greater than that calculated on the basis of atypical tracer m/z 147. Although the tracer and PMF approaches can at times agree (Kroll, 2014) and the tracer and molecular-ion approaches can sometimes agree as well (Smith et al., 2009), our results suggest that the heterogeneous kinetics of OA is underestimated when a non-molecular ion peak is

used as the tracer to measure the particle phase concentration of OA based on UMR-AMS. In model simulations, the reactive uptake coefficient of OH or other radicals, which are calculated based upon k_2, is an important parameter in evaluating the fate of OA during transport. The current results suggest that the lifetime of OA estimated in models due to heterogeneous oxidation might be overestimated for a reaction system where the products are highly similar to the reactant and the kinetic data are derived by individual non-molecular m/z tracers of OA. The results also suggest that it may be necessary to revisit the kinetic data of other organic aerosol components (and OH uptake coefficients) which have been derived using the relative rates technique (George et al., 2007;Lambe et al., 2007) based on UMR-AMS. Finally, these results imply that the heterogeneous oxidation of aerosols will be dependent upon a number of factors related to the reaction system, and that a single rate constant for one system cannot be universally applied under all conditions. Future work is thus required to elucidate the chemical and physical parameters which control the OH heterogeneous reaction kinetics and the associated need to apply PMF for a variety of chemical systems. This may be best accomplished through systematic application of the PMF approach to species with differing mass spectral characteristics, such as linear/branched alkanes, monocarboxylic acids and other oxygenates. As illustrated in this study, the kinetics derived with PMF may differ from that derived with tracer ions, with both based upon EI-AMS approaches. This highlights the usefulness of measurements from CIMS, GC-MS and VUV-AMS, for the determination of heterogeneous loss rates, since these instruments are more likely to retain the reactant

522 molecular information.

523

524 **Supporting Information**

525 Supplementary material related to this article is available online at:

526

527 **Acknowledgements**

528 This research was funded by the Chemicals Management Plan (CMP) and the Clean

529 Air Regulatory Agenda (CARA).

530 **Literature Cited:**

531 Allan, J. D., Jimenez, J. L., Williams, P. I., Alfarra, M. R., Bower, K. N., Jayne, J. T., Coe, H., and
532 Worsnop, D. R.: Quantitative sampling using an Aerodyne aerosol mass spectrometer 1. Techniques of
533 data interpretation and error analysis, J. Geophys. Res., 108, 4090, 10.1029/2002jd002358, 2003.
534 Atkinson, R.: Kinetics and Mechanisms of the Gas-Phase Reactions of the Hydroxyl Radical with
535 Organic Compounds under Atmospheric Conditions, Chem. Rev., 85, 69-201, 1986.
536 Atkinson, R., and Arey, J.: Atmospheric Degradation of Volatile Organic Compounds, Chem. Rev., 103,
537 4605-4638, 2003.
538 Cappa, C. D., Che, D. L., Kessler, S. H., Kroll, J. H., and Wilson, K. R.: Variations in organic aerosol
539 optical and hygroscopic properties upon heterogeneous OH oxidation, J. Geophys. Res., 116, D15204,
540 10.1029/2011jd015918, 2011.
541 Che, D. L., Smith, J. D., Leone, S. R., Ahmed, M., and Wilson, K. R.: Quantifying the reactive uptake
542 of OH by organic aerosols in a continuous flow stirred tank reactor, Phys. Chem. Chem. Phys., 11,
543 7885-7895, 10.1039/b904418c, 2009.
544 Donahue, N. M., Robinson, A. L., Hartz, K. E. H., Sage, A. M., and Weitkamp, E. A.: Competitive
545 oxidation in atmospheric aerosols: The case for relative kinetics, Geophys. Res. Lett., 32, L16805,
546 10.1029/2005gl022893, 2005.
547 Drewnick, F., Hings, S. S., DeCarlo, P., Jayne, J. T., Gonin, M., Fuhrer, K., Weimer, S., Jimenez, J. L.,
548 Demerjian, K. L., Borrmann, S., and Worsnop, D. R.: A New Time-of-Flight Aerosol Mass
549 Spectrometer (TOF-AMS)—Instrument Description and First Field Deployment, Aerosol Sci. Technol.,
550 39, 637-658, 2005.
551 Fuchs, N. A., and Sutugin, A. G.: Highly Dispersed Aerosols, Butterworth-Heinemann, Newton, MA,
552 1970.
553 George, I. J., Vlasenko, A., Slowik, J. G., Broekhuizen, K., and Abbatt, J. P. D.: Heterogeneous
554 oxidation of saturated organic aerosols by hydroxyl radicals: uptake kinetics, condensed-phase products,
555 and particle size change, Atmos. Chem. Phys., 7, 4187-4201, 2007.
556 George, I. J., and Abbatt, J. P. D.: Chemical evolution of secondary organic aerosol from OH-initiated

heterogeneous oxidation, Atmos. Chem. Phys., 10, 5551-5563, 2010.
Hearn, J. D., and Smith, G. D.: A mixed-phase relative rates technique for measuring aerosol reaction kinetics, Geophys. Res. Lett., 33, L17805, 10.1029/2006gl026963, 2006.
Huisman, A. J., Krieger, U. K., Zuend, A., Marcolli, C., and Peter, T.: Vapor pressures of substituted polycarboxylic acids are much lower than previously reported, Atmos. Chem. Phys., 13, 6647-6662, 10.5194/acp-13-6647-2013, 2013.
Isaacman, G., Chan, A. W. H., Nah, T., Worton, D. R., Ruehl, C. R., Wilson, K. R., and Goldstein, A. H.: Heterogeneous OH Oxidation of Motor Oil Particles Causes Selective Depletion of Branched and Less Cyclic Hydrocarbons, Environ. Sci. Technol., 46, 10632-10640, 10.1021/es302768a, 2012.
Jacobson, M. Z.: Fundamentals of Atmospheric Modeling, Cambridge University Press, 2005.
Jayne, J. T., Leard, D. C., Zhang, X., Davidovits, P., Smith, K. A., Kolb, C. E., and R.Worsnop, D.: Development of an Aerosol Mass Spectrometer for Size and Composition Analysis of Submicron Particles, Aerosol Sci. Technol., 33, 49-70, 2000.
Kessler, S. H., Smith, J. D., Che, D. L., Worsnop, D. R., Wilson, K. R., and Kroll, J. H.: Chemical Sinks of Organic Aerosol: Kinetics and Products of the Heterogeneous Oxidation of Erythritol and Levoglucosan, Environ. Sci. Technol., 44, 7005-7010, 10.1021/es101465m, 2010.
Kessler, S. H., Nah, T., Daumit, K. E., Smith, J. D., Leone, S. R., Kolb, C. E., Worsnop, D. R., Wilson, K. R., and Kroll, J. H.: OH-Initiated Heterogeneous Aging of Highly Oxidized Organic Aerosol, J. Phys. Chem. A, 116, 6358-6365, 10.1021/jp212131m, 2012.
Kolb, C. E., Cox, R. A., Abbatt, J. P. D., Ammann, M., Davis, E. J., Donaldson, D. J., Garrett, B. C., George, C., Griffiths, P. T., Hanson, D. R., Kulmala, M., McFiggans, G., P¨oschl, U., Riipinen, I., Rossi, M. J., Rudich, Y., Wagner, P. E., Winkler, P. M., Worsnop, D. R., and Dowd, C. D. O.: An overview of current issues in the uptake of atmospheric trace gases by aerosols and clouds, Atmos. Chem. Phys. , 10, 10561-10605, 2010.
Kroll, J. H., and Seinfeld, J. H.: Chemistry of secondary organic aerosol: Formation and evolution of low-volatility organics in the atmosphere, Atmos. Environ., 42, 3593-3624, 2008.
Lambe, A. T., Zhang, J. Y., Sage, A. M., and Donahue, N. M.: Controlled OH radical production via ozone-alkene reactions for use in aerosol aging studies, Environ. Sci. Technol., 41, 2357-2363, 10.1021/es061878e, 2007.
Lambe, A. T., Miracolo, M. A., Hennigan, C. J., Robinson, A. L., and Donahue, N. M.: Effective Rate Constants and Uptake Coefficients for the Reactions of Organic Molecular Markers (n-Alkanes, Hopanes, and Steranes) in Motor Oil and Diesel Primary Organic Aerosols with Hydroxyl Radicals, Environ. Sci. Technol., 43, 8794-8800, 10.1021/es901745h, 2009.
Li, P., Al-Abadleh, H. A., and Grassian, V. H.: Measuring heterogeneous uptake coefficients of gases on solid particle surfaces with a Knudsen Cell reactor: complications due to surface saturation and gas diffusion into underlying layers., J. Phys. Chem. A., 106, 1210-1219, 2002.
Liggio, J., Li, S. M., Vlasenko, A., Sjostedt, S., Chang, R., Shantz, N., Abbatt, J., Slowik, J. G., Bottenheim, J. W., Brickell, P. C., Stroud, C., and Leaitch, W. R.: Primary and secondary organic aerosols in urban air masses intercepted at a rural site, J. Geophys. Res.-Atmos., 115, D21305, doi:21310.21029/22010JD014426., D21305
10.1029/2010jd014426, 2010.
Liu, C., Zhang, P., Wang, Y., Yang, B., and Shu, J.: Heterogeneous Reactions of Particulate Methoxyphenols with NO3 Radicals: Kinetics, Products, and Mechanisms, Environ. Sci. Technol., 46, 13262-13269, 2012.

Liu, Y., Liggio, J., Harner, T., Jantunen, L., Shoeib, M., and Li, S.-M.: Heterogeneous OH initiated oxidation: A possible explanation for the persistence of organophosphate flame retardants in air, Environ. Sci. Technol., 48, 1041-1048, 2014.

Ma, J., Liu, Y., and He, H.: Degradation kinetics of anthracene by ozone on mineral oxides, Atmos. Environ. , 44, 4446-4453, 2010

McNeill, V. F., Wolfe, G. M., and Thornton, J. A.: The Oxidation of Oleate in Submicron Aqueous Salt Aerosols: Evidence of a Surface Process, J. Phys. Chem. A, 111, 1073-1083, 2007.

McNeill, V. F., Yatavelli, R. L. N., Thornton, J. A., Stipe, C. B., and Landgrebe, O.: Heterogeneous OH oxidation of palmitic acid in single component and internally mixed aerosol particles: vaporization and the role of particle phase, Atmos. Chem. Phys., 8, 5465-5476, 10.5194/acp-8-5465-2008, 2008.

Norris, G., and Vedantham, R.: EPA positive matrix factorization (PMF) 3.0 fundamentals & user guide, U.S. Environmental Protection Agency, www.epa.gov, 2008.

Pöschl, U.: Atmospheric Aerosols: Composition, Transformation, Climate and Health Effects, Angew. Chem. Int. Ed., 44, 7520-7540, 2005.

Paatero, P., and Tapper, U.: Positive matrix factorization: a nonnegative factor model with optimal utilization of error estimates of data values, Environmetrics 5, 111-126, 1994.

Paatero, P.: Least squares formulation of robust non‐negative factor analysis, Chemom. Intell. Lab. Syst., 37, 23-35, doi:10.1016/S0169-7439(96)00044-5., 1997.

Paatero, P., and Hopke, P. K.: Discarding or downweighting highnoise variables in factor analytic models, Anal. Chim. Acta, 490, 277-289, 2003.

Pankow, J. F.: An absorption-model of gas-particle partitioning of organic compounds in the atmosphere, Atmos. Environ., 28, 185-188, 1994.

Price, H. C., Murray, B. J., Mattsson, J., O'Sullivan, D., Wilson, T. W., Baustian, K. J., and Benning, L. G.: Quantifying water diffusion in high-viscosity and glassy aqueous solutions using a Raman isotope tracer method, Atmos. Chem. Phys., 14, 3817-3830, 10.5194/acp-14-3817-2014, 2014.

Reff, A., Eberly, S. I., and Bhave, P. V.: Receptor modeling of ambient particulate matter data using positive matrix factorization: Review of existing methods, J. Air Waste Manage., 57, 146-154, 2007.

Renbaum, L. H., and Smith, G. D.: Artifacts in measuring aerosol uptake kinetics: the roles of time, concentration and adsorption, Atmos. Chem. Phys., 11, 6881-6893, 10.5194/acp-11-6881-2011, 2011.

Sareen, N., Moussa, S. G., and McNeill, V. F.: Photochemical Aging of Light-Absorbing Secondary Organic Aerosol Material, J. Phys. Chem. A, 117, 2987-2996, 2013.

Schwartz, R. E., Russell, L. M., Sjostedt, S. J., Vlasenko, A., Slowik, J. G., Abbatt, J. P. D., Macdonald, A. M., Li, S. M., Liggio, J., Toom-Sauntry, D., and Leaitch, W. R.: Biogenic oxidized organic functional groups in aerosol particles from a mountain forest site and their similarities to laboratory chamber products, Atmos. Chem. Phys., 10, 5075-5088, 10.5194/acp-10-5075-2010, 2010.

Slowik, J. G., Wong, J. P. S., and Abbatt, J. P. D.: Real-time, controlled OH-initiated oxidation of biogenic secondary organic aerosol, Atmos. Chem. Phys., 12, 9775-9790, 10.5194/acp-12-9775-2012, 2012.

Smith, J. D., Kroll, J. H., Cappa, C. D., Che, D. L., Liu, C. L., Ahmed, M., Leone, S. R., Worsnop, D. R., and Wilson, K. R.: The heterogeneous reaction of hydroxyl radicals with sub-micron squalane particles: a model system for understanding the oxidative aging of ambient aerosols, Atmos. Chem. Phys., 9, 3209-3222, 10.5194/acp-9-3209-2009, 2009.

Song, Y., Zhang, Y., Xie, S., Zeng, L., Zheng, M., Salmon, L. G., Shao, M., and Slanina, S.: Source apportionment of PM2.5 in Beijing by positive matrix factorization, Atmos. Environ., 40, 1526-1537,

2006.
Ulbrich, I. M., Canagaratna, M. R., Zhang, Q., Worsnop, D. R., and Jimenez, J. L.: Interpretation of organic components from Positive Matrix Factorization of aerosol mass spectrometric data, Atmos. Chem. Phys., 9, 2891-2918, 2009.
Viana, M., Kuhlbusch, T. A. J., Querol, X., Alastuey, A., Harrison, R. M., Hopke, P. K., Winiwarter, W., Vallius, A., Szidat, S., Prevot, A. S. H., Hueglin, C., Bloemen, H., Wahlin, P., Vecchi, R., Miranda, A. I., Kasper-Giebl, A., Maenhaut, W., and Hitzenberger, R.: Source apportionment of particulate matter in Europe: A review of methods and results, J. Aerosol. Sci., 39, 827-849, 10.1016/j.jaerosci.2008.05.007, 2008.
Weitkamp, E. A., Hartz, K. E. H., Sage, A. M., Donahue, N. M., and Robinson, A. L.: Laboratory measurements of the heterogeneous oxidation of condensed-phase organic molecular makers for meat cooking emissions, Environ. Sci. Technol., 42, 5177-5182, 2008a.
Weitkamp, E. A., Lambe, A. T., Donahue, N. M., and Robinson, A. L.: Laboratory Measurements of the Heterogeneous Oxidation of Condensed-Phase Organic Molecular Makers for Motor Vehicle Exhaust, Environ. Sci. Technol., 42, 7950-7956, 10.1021/es800745x, 2008b.
Widmann, J. F., and Davis, E. J.: Mathematical models of the uptake of ClONO2 and other gases by atmospheric aerosols, J. Aerosol. Sci., 28, 87-106, 1997.
Wilson, K. R., Smith, J. D., Kessler, S. H., and Kroll, J. H.: The statistical evolution of multiple generations of oxidation products in the photochemical aging of chemically reduced organic aerosol, Phys. Chem. Chem. Phys., 14, 1468-1479, 10.1039/c1cp22716e, 2012.
Worsnop, D. R., Morris, J. W., Shi, Q., Davidovits, P., and Kolb, C. E.: A chemical kinetic model for reactive transformations of aerosol particles, Geophys. Res. Lett., 29, 1996, 10.1029/2002gl015542, 2002.
Yuan, Z. B., Yu, J. Z., Lau, A. K. H., Louie, P. K. K., and Fung, J. C. H.: Application of positive matrix factorization in estimating aerosol secondary organic carbon in Hong Kong and its relationship with secondary sulfate, Atmos. Chem. Phys., 6, 25-34, 10.5194/acp-6-25-2006, 2006.
Zhang, Q., Jimenez, J., Canagaratna, M., Ulbrich, I., Ng, N., Worsnop, D., and Sun, Y.: Understanding atmospheric organic aerosols via factor analysis of aerosol mass spectrometry: a review, Anal. Bioanal. Chem., 401, 3045-3067, 10.1007/s00216-011-5355-y, 2011.

689 **Table 1.** Comparison of the measured k_2 values utilizing PMF and select m/z tracers,

690 for organophosphate compounds and CA.

OA	Mean k_{r_PMF}	k_2 (10^{12}) cm^3 molecule^{-1} s^{-1}			k_{2_PMF}/ k_{2_Tracer}	M_{Tracer}/M^+
		$k_{2,\ obs\_PMF}$	$k_{2,\ t\ \_PMF}$	$k_{2,\ t\ \_Tracer}$		
TPhP	1.58±0.33	1.48±0.31	1.95±0.43	2.10±0.19[a]	0.9	326/326
TDCPP	1.20±0.31	1.13±0.29	1.35±0.35	0.92±0.09[a]	1.5	381/431
TEHP	3.52±0.65	3.31±0.61	4.25±0.78	2.70±0.63[a]	1.6	323/435
CA	3.01±0.27	2.83±0.25	3.31±0.29	0.79±0.06	4.2	147/192

691 a.(Liu et al., 2014)

692

693

694

695

696

697

698

699

700

701

702

703

704

705

706

707

Figure captions

Figure 1. Changes in (A) total organic mass concentration, (B) the fraction of unreacted citric acid derived by PMF and (C) products of citric acid oxidized by OH derived by PMF, as a function of relative experimental time. The values 1 – 6 represent a step-wise O_3 concentration decrease, corresponding to decreased OH exposure; 0 represents an O_3 concentration of zero. Experimental conditions are D_m: 200 nm, RH: 30±3 %, T: 298 K.

Figure 2. Normalized mass spectra of (A) citric acid (PMF factor 1), (B) citric acid oxidation products (PMF factor 2), and (C) the difference mass spectrum (Factor 2 – Factor 1). The numbers in the upper two rows are the intensities of m/z 87 and 129, while negative values are shown in the bottom row. The red and green lines indicate a negative and positive value, respectively.

Figure 3. Mass spectra (A) of CA from NIST database, (B) of pure CA measured with the C-ToF-AMS.

Figure 4. Comparison between the mass spectra of factor 1 from PMF analysis and pure CA directly measured by the C-ToF-AMS. The inset graph is the correlation of their corresponding signal intensities.

Figure 5. Changes in the relative concentration of (A) methanol, (B) citric acid extracted with PMF analysis and (C) specific tracers measured with the AMS during the OH initiated oxidation of citric acid. Experimental conditions are D_m: 140 nm, RH: 30±3 %, T: 298 K. The values in the top row represent the OH exposures.

Figure 6. Relative concentration of citric acid (c/c_0) as a function of the relative concentration of methanol based upon (A) PMF analysis, (B) m/z=129 and (C) m/z

147. Experimental conditions are D_m: 140 nm, RH: 30±3 %, T: 298 K.

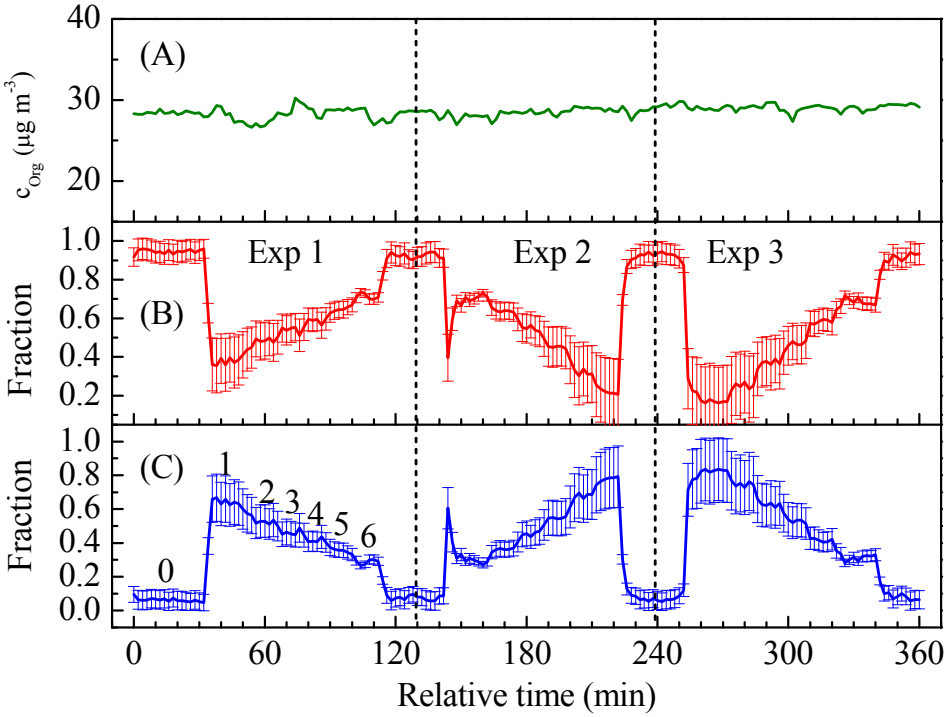

744

745 **Figure 1**.

746

747

748

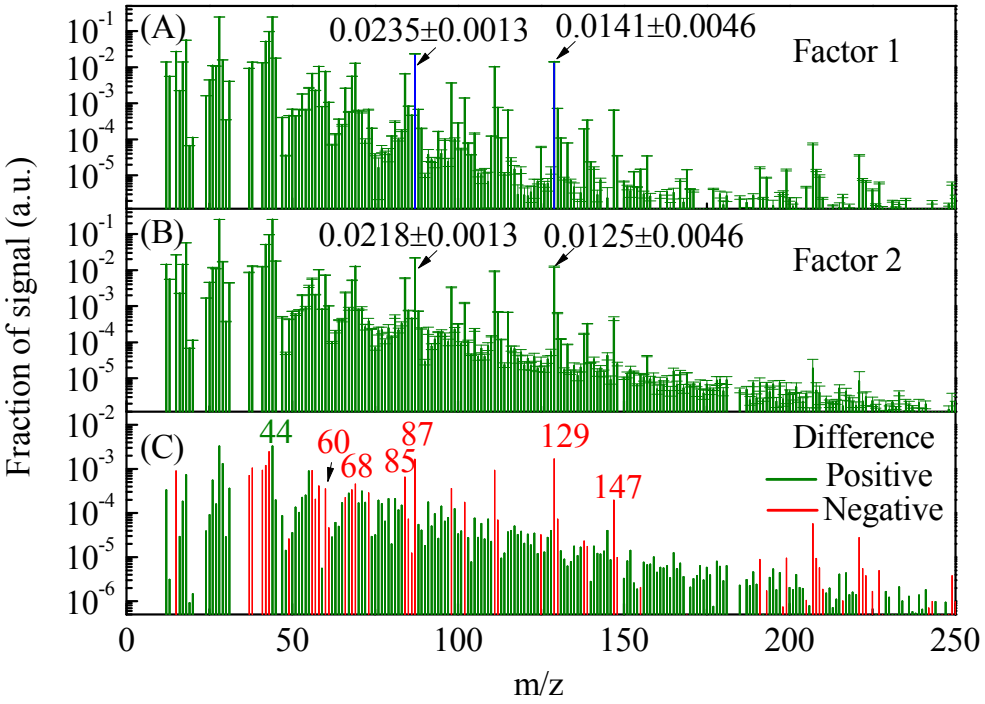

749

750 **Figure 2.**

751

752

753

754

755

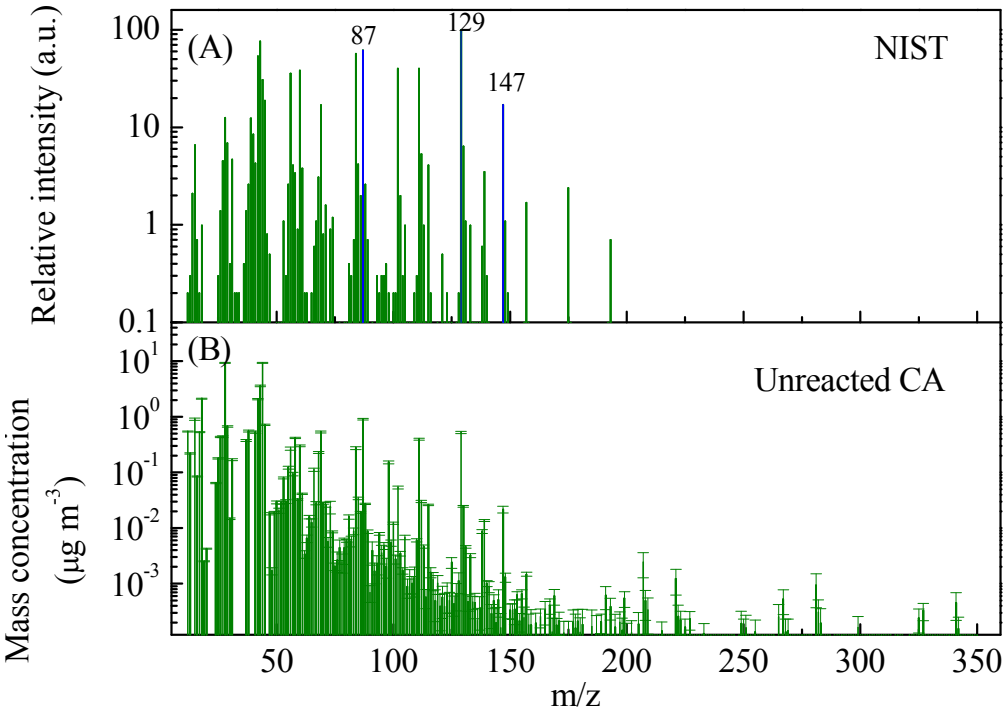
(A)
NIST
87
129
147
Relative intensity (a.u.)
100
10
1
0.1
(B)
Unreacted CA
Mass concentration
(μg m-3)
10^1
10^0
10^-1
10^-2
10^-3
50
100
150
200
250
300
350
m/z

Figure 3.

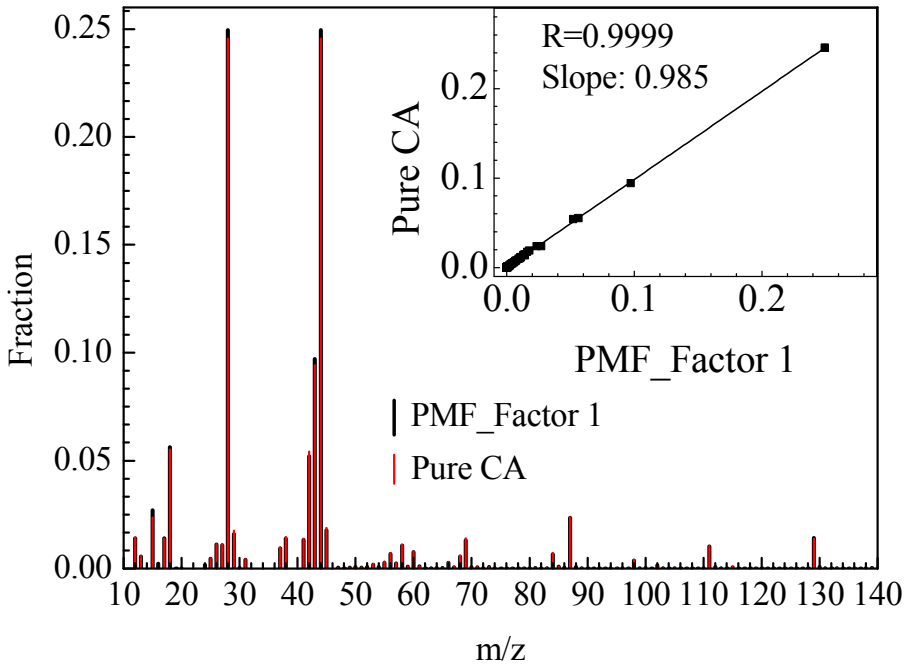

770

771 **Figure 4.**

772

773

774

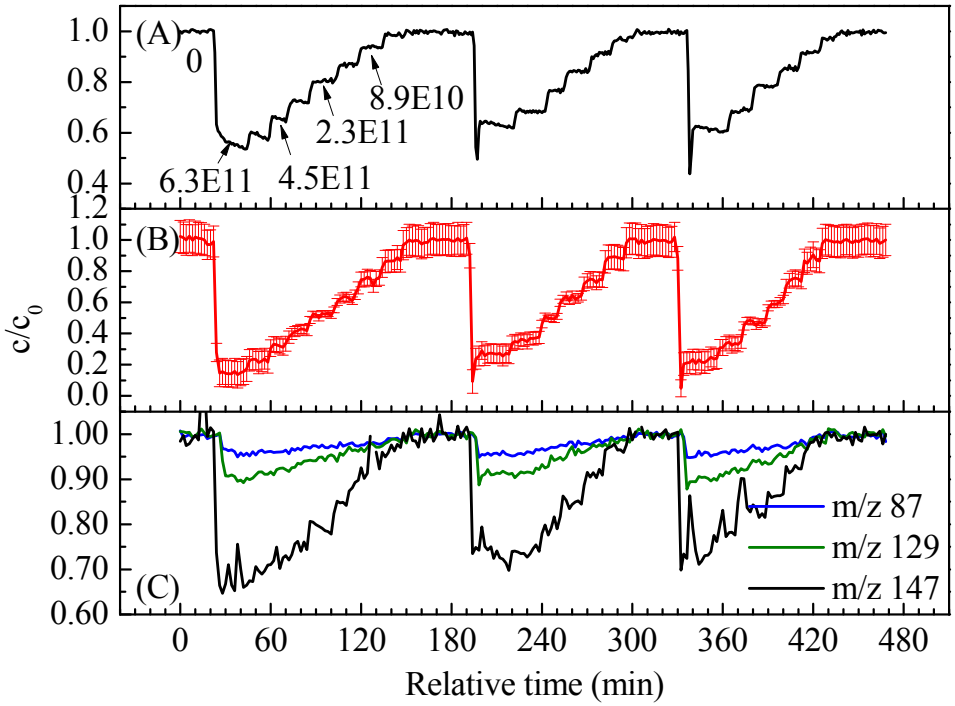

775

776 **Figure 5.**

777

778

779

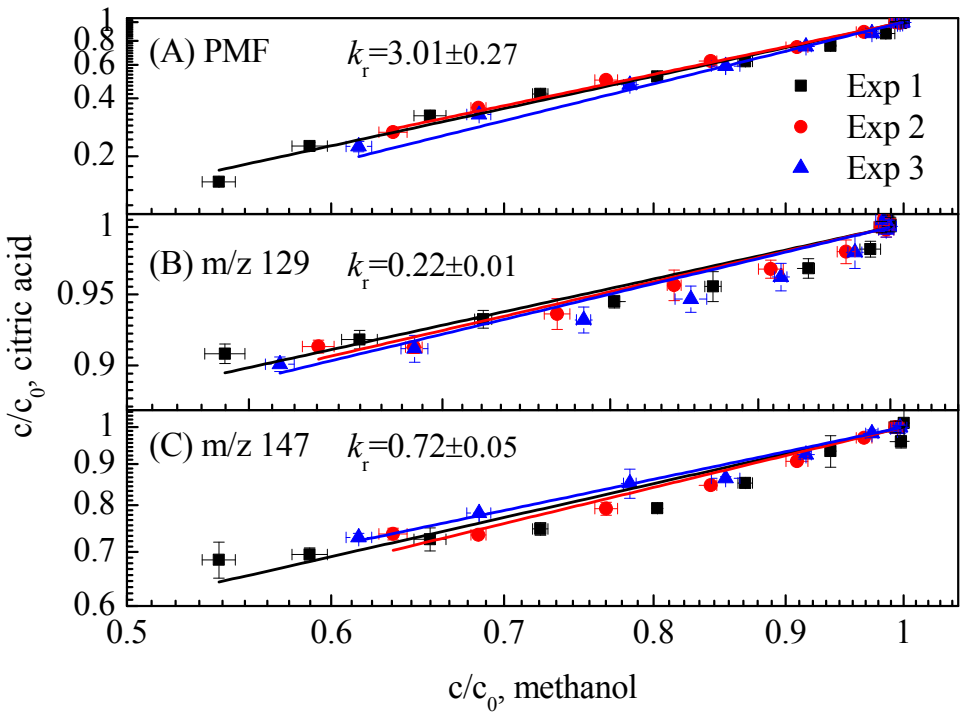

780

781 **Figure 6.**

782